Materials Transactions, JIM, Vol. 38, No. 10 (1997), pp. 821 to 835

OVERVIEW

High-Temperature Oxidation of Silicon Carbide and Silicon Nitride

T. Narushima*, T. Goto**, T. Hirai**
and Y. Iguchi*

*Department of Metallurgy, Faculty of Engineering, Tohoku University, Sendai 980-77, Japan
**Institute for Materials Research, Tohoku University, Sendai 980-77, Japan

Oxidation behavior of silicon-based ceramics such as SiC and Si_3N_4 at high temperatures is important for their practical applications to structural or electronic materials. In the present paper two kinds of oxidation (passive and active) and active-to-passive transition of silicon-based ceramics were discussed thermodynamically, and the rate constants of passive/active oxidation and active-to-passive transition oxygen potentials for SiC and Si_3N_4 were reviewed. Passive and active oxidation behavior depended on the microstructure of oxide films and SiO gas pressure on silicon-based ceramics, respectively. Wagner model, volatility diagram and solgasmix-based calculation were used to estimate the active-to-passive transition.

(Received June 10, 1997)

Keywords: *silicon carbide, silicon nitride, silicon-based ceramics, oxidation, high-temperature, silica, passive oxidation, active oxidation, transition*

I. Introduction

Silicon-based ceramics such as silicon carbide (SiC) and silicon nitride (Si_3N_4) are expected to be structural materials at high temperatures because of their superior chemical and physical stability and mechanical properties[1)-23)]. The environmental conditions in which silicon-based ceramics will be applied are severe. Therefore, the use of silicon-based ceramics is affected by their oxidation resistance at high temperatures. SiC is an attractive material for semiconductor devices such as diodes or transistors[24)-32)], and the thermally formed SiO_2 layer on SiC during oxidation is used as a mask material or a gate dielectric. Si_3N_4 has been widely used as local oxidation masks and surface passivation films in semiconductor devices because of its higher stability than silica[33)]. Thus, the oxidation resistance is important for the application of SiC and Si_3N_4 to structural or electronic materials. Silicon-based ceramics exhibit two types of oxidation behavior, passive and active oxidation, depending on oxygen partial pressure and temperature[34)35)]. The passive oxidation is observed under high oxygen partial pressures, in which a protective SiO_2 film prevents further oxidation. Passive oxidation reaction of SiC and Si_3N_4 with oxygen gas can be expressed by eqs. (1) and (2), respectively.

$$SiC(s)+3/2O_2(g)=SiO_2(s)+CO(g) \quad (1)$$

$$Si_3N_4(s)+3O_2(g)=3SiO_2(s)+2N_2(g) \quad (2)$$

Active oxidation occurs at low oxygen partial pressures. In active oxidation no protective films are expected because of significant SiO vapor formation (eqs. (3) and (4)).

$$SiC(s)+O_2(g)=SiO(g)+CO(g) \quad (3)$$

$$Si_3N_4(s)+3/2O_2(g)=3SiO(g)+2N_2(g) \quad (4)$$

Passive and active oxidation lead to mass gain and mass loss, respectively.

Silicon-based ceramics have been noted as superior structural materials in 1950's, and the passive and active oxidation of these materials have been investigated[36)-39)]. Schlichting[40)41)] reviewed the passive/active oxidation rates of SiC. Recent topics relating to the oxidation of silicon-based ceramics have been reviewed by Jacobson[42)].

In the present paper, first of all active-to-passive transition was dealt with, and then passive oxidation and active oxidation of SiC and Si_3N_4 were reviewed. SiO_2 films formed during oxidation do not always mean protective. In this paper, however, the oxidation with SiO_2 formation and the mass gain is called "passive", and the oxidation with gaseous SiO formation and the mass loss is called "active".

II. Active-to-Passive Transition of Silicon-Based Ceramics

Figure 1 demonstrates the potential diagram of Si–C–N–O system at 1873 K calculated using the thermodynamic data[43)]. Passive oxidation may be expected above the equilibrium oxygen pressure at which SiO_2 and SiC (or

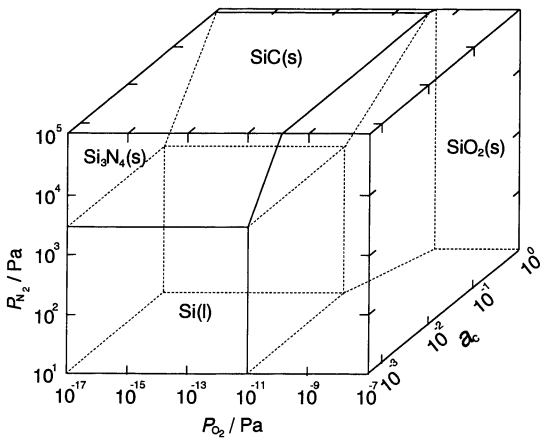

Fig. 1 Potential diagram of Si-C-N-O system at 1873 K.

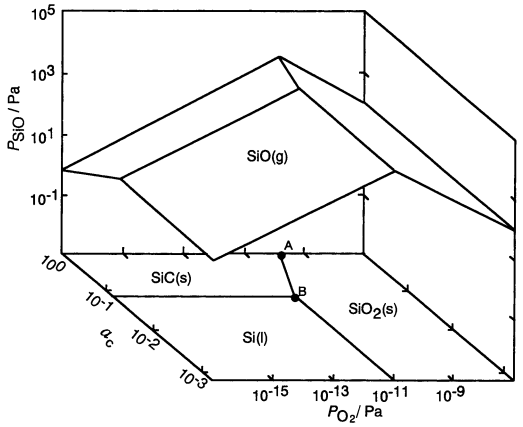

Fig. 2 Equilibrium SiO partial pressure in Si-C-O system at 1873 K.

Si_3N_4) phases coexist. In practice, oxidation behavior is complicated by the presence of gaseous SiO. Equilibrium SiO partial pressure in the Si-C-O system at 1873 K is shown in Fig. 2. The maximum SiO partial pressure is around 10 kPa which is much higher than the equilibrium oxygen pressure represented by the line AB in Fig. 2. Therefore, when the rate of oxygen consumption by eq. (3) is higher than that of oxygen supply by diffusion in gas phase, a gaseous boundary layer of oxygen gas may be formed on the surface of SiC and the active oxidation occurs.

Since the active oxidation resulting in significant mass loss often leads to the degradation of mechanical properties[44][45], it is essential to clarify the active oxidation region. In this section, the estimation of active-to-passive transition will be discussed. The oxygen partial pressure for the active-to-passive transition is reviewed in later sections (III-2 and IV-2) together with active oxidation.

The models for the active-to-passive transition proposed by Wagner[46] and Turkdogan *et al.*[47] are well known. Figure 3 demonstrates the gas pressure profiles in both of the models. Vaporization of metal (M) affects the transition in Turkdogan model. Metal oxide smoke (fog) is formed by the reaction of metal vapor and oxygen (eq. (5)).

$$M(g)+O_2(g)=MO_2(s) \tag{5}$$

The distance δ through which the metal vapor is transported decreases with increasing ambient oxygen partial pressure ($P^b_{O_2}$). Turkdogan *et al.*[47] assumed that the active-to-passive transition occurred when δ approached the mean free path of the metal oxide smoke. The active-to-passive transition oxygen partial pressure ($P^t_{O_2}$) can be represented by eq. (6).

$$P^t_{O_2}=(P^s_M/h_{O_2})(RT/2\pi M_M)^2 \tag{6}$$

where h_{O_2} and M_M are mass-transfer coefficient of oxygen and atomic mass of the metal vapor, respectively. For silicon-based ceramics this mechanism seems unlikely because of the low vapor pressure of the relevant components (i.e., silicon, carbon or nitrogen). Wagner presented a model in which a gaseous boundary layer (i.e.,

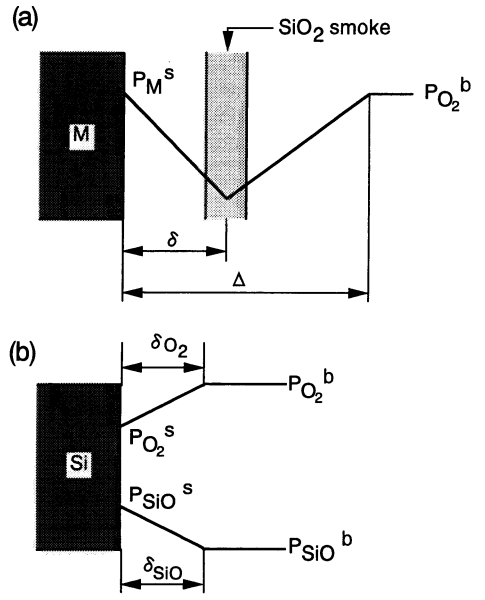

Fig. 3 Pressure profiles of O_2 and SiO for (a) Turkdogan model and (b) Wagner model.

$P^b_{O_2} \gg P^s_{O_2}$ and $P^s_{SiO} \gg P^b_{SiO}$ in Fig. 3(b)) was assumed in order to interpret the active-to-passive transition of silicon in an inert gas-oxygen atmosphere. $P^t_{O_2}$ for SiC in an inert gas-oxygen atmosphere can be expressed by eq. (7).

$$P^t_{O_2}=(D_{SiO}/D_{O_2})^{1/2}P^{eq}_{SiO} \tag{7}$$

where D_i is the diffusivity of i in gas phase and P^{eq}_{SiO} is the equilibrium SiO partial pressure of eq. (8).

$$SiC(s)+2SiO_2(s)=3SiO(g)+CO(g) \tag{8}$$

The model which took account of the presence of liquid SiO was presented by Nickel[48]. The presence of condensed SiO phase[49], however, has not been confirmed experimentally up to now[50]. Heuer *et al.*[51]-[53] proposed a volatility diagram by which the active-to-passive transition could well be understood. Figure 4 demonstrates the volatility diagram in $SiC-O_2-Ar$ system at 1873 K. The volatility diagram indicates a vapor pressure of the most volatile species at a given oxygen potential together with

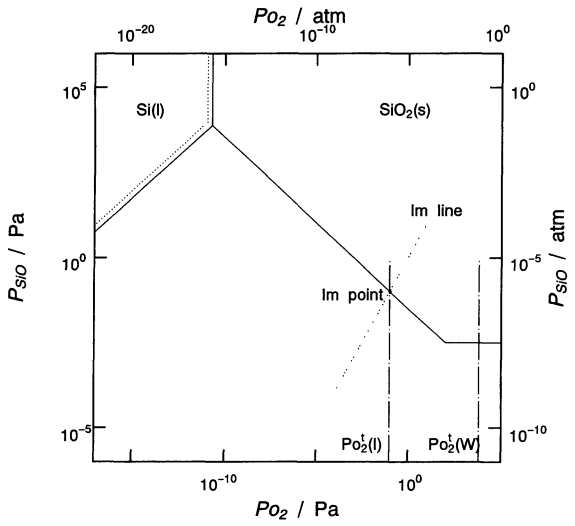

Fig. 4 Volatility diagram of SiC-O_2-Ar system at 1873 K.

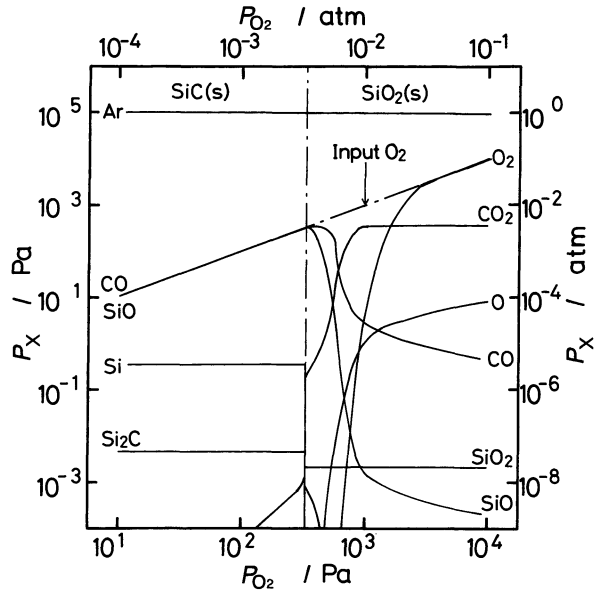

Fig. 5 Equilibrium partial pressures of gas species produced by the reaction of SiC in Ar-O_2 atmospheres at 1873 K.

stable condensed phase. The dotted line in Fig. 4 is called "isomolar (Im) line" on which $P_{O_2}=P_{SiO}$ is satisfied, i.e., the line shows the mass balance for eq. (3). $P^t_{O_2}(W)$ in Fig. 4 means the calculated $P^t_{O_2}$ value from eq. (7). Heuer *et al.* have pointed out that the active-to-passive transition is possible between $P^t_{O_2}(I)$ and $P^t_{O_2}(W)$, because SiO gas formed must be oxidized to SiO_2 smoke (fog) in the gas phase (eq. (9)) just above the SiC surface at oxygen partial pressures higher than $P^t_{O_2}(I)$, and then the SiO_2 smoke might deposited on the SiC surface.

$$SiO(g)+1/2O_2(g)=SiO_2(s,\ smoke) \qquad (9)$$

Heuer *et al.* assumed that the rate-controlling step of the active oxidation is oxygen diffusion through a gaseous boundary layer, and can well explain the active-to-passive transition for silicon-based ceramics.

It is useful to estimate the $P^t_{O_2}$ value in the complex atmosphere containing a number of gas species. The authors estimated the $P^t_{O_2}$ value for SiC and Si_3N_4 by using computer program SAGE[54] which minimizes the free energy under mass balance conditions[55]-[57]. The chemical species used in the calculation are listed in Table 1. Figure 5 demonstrates the thermodynamically calculated results using SAGE, where stable solid phases and partial pressures of gas species for the SiC-O_2-Ar system are indicated. The SiO partial pressure decreased abruptly with changing of the stable solid phase from SiC to SiO_2, indicating the occurrence of the active-to-passive transition. The oxygen partial pressure at which the change occurred agreed well with the experimentally measured $P^t_{O_2}$ value[55].

Table 1 Chemical species in the Si-C-N-O system.

(Gas species)						
C	CN	CNO	CNN	NCN	CO	CO_2
SiC	Si_2C	C_2	C_2N	C_2N_2	C_2O	SiC_2
C_3	C_3O_2	C_4	C_4N_2	C_5	N	NO
NO_2	NO_3	SiN	Si_2N	N_2	N_2O	N_2O_3
N_2O_4	N_3	O	SiO	O_2	SiO_2	O_3
Si	Si_2	Si_3	Ar			
(Condensed species)						
C	Si	SiC	N_2O_4	Si_3N_4	SiO_2	

III. Oxidation of SiC

1. Passive oxidation

The studies on passive oxidation in dry and wet atmospheres and active oxidation of SiC are summarized in Tables 2[58]-[66], 3[67]-[75] and 4[44][55][58][76]-[88], respectively. The data on the highly pure and dense sample, single crystal (SC) or chemically vapor deposited (CVD) SiC, are shown in Table 2.

The oxidation mechanism in a dry atmosphere can be explained in terms of parabolic or linear-parabolic mechanism below the melting point of cristobalite (2001 K[89]). The values of parabolic rate constant (k_p) of SC and CVD-SiC are compared with those of hot-pressed (HP)[62][90]-[92] and pressureless sintered (PLS)[62][93] SiC in Fig. 6. This figure shows that the oxidation resistance of SC and CVD-SiC is superior to that of HP and PLS-SiC, and the k_p values of SC and CVD-SiC are within one order of magnitude except those of controlled nucleation thermally deposited (CNTD) SiC containing silicon as an impurity[62]. These results suggest that the oxidation is accelerated by impurities or sintering additives in the body which affect the microstructure of a protective silica film[90]. For instance the oxidation rate of HP-SiC containing Al_2O_3 as a sintering additive increases dramatically above the eutectic point[94] between mullite and silica owing to the formation of the liquid phase. On the other hand, dense and smooth amorphous SiO_2 or cristobalite protective film can be formed on SC and CVD-SiC. The crystallization rate from amorphous SiO_2 to cristobalite

Table 2 Passive oxidation of SiC in dry atmospheres.

Author (year) [Ref. No.]	Method	Type of SiC	Atmosphere	Temperature (K)	Time (ks)	Kinetics	Activation energy ($kJ \cdot mol^{-1}$)
Gulbransen *et al.* (1966) [58]	Thermogravimetry	Single crystal (α, 6H)	O_2 (P_{total}=1.2–66 Pa)	1423–1623	3.6	0–0.3 ks: Linear (1523 K, 5.3 Pa: 7.5×10^{-5} $kg\cdot m^{-2}\cdot s^{-1}$) 0.3–3.6 ks: Parabolic (?)	
Bartlett (1971) [59]	Interferometry	Single crystal (β)	O_2, 0.1 MPa	1253–1273	167.4	Parabolic 1258 K: 2.9×10^{-18} $m^2\cdot s^{-1}$ 1273 K: 2.0×10^{-18} $m^2\cdot s^{-1}$	
Harris and Call (1974) [60]	Interferometry	Single crystal (α, 6H)	O_2, 0.1 MPa	1243–1518	1209.6	Thick oxide side: Linear-parabolic k_p 1243 K: 4.1×10^{-19} $m^2\cdot s^{-1}$ 1518 K: 6.0×10^{-18} $m^2\cdot s^{-1}$ Thin oxide side: Linear k_l 1243 K: 3.7×10^{-14} $m\cdot s^{-1}$ 1518 K: 1.9×10^{-11} $m\cdot s^{-1}$	Thick oxide side k_p: 197 Thin oxide side k_l: 356
Kossowski and Singhal (1975) [61]	Thermogravimetry	CVD	O_2, 0.1 MPa	1643	86.4	Parabolic 1.1×10^{-11} $kg^2\cdot m^{-4}\cdot s^{-1}$	
Costello and Tressler (1986) [62]	Ellipsometry Profilometry	CVD (CNTD) (+Si)	O_2, 0.1 MPa	1473–1773	7.2	Parabolic 1473 K: 5.7×10^{-18} $m^2\cdot s^{-1}$ 1773 K: 7.5×10^{-17} $m^2\cdot s^{-1}$	142–293
Costello and Tressler (1986) [62]	Ellipsometry Profilometry	Single crystal (α, black)	O_2, 0.1 MPa	1473–1773	7.2	Parabolic C face 1473 K: 4.7×10^{-18} $m^2\cdot s^{-1}$ 1773 K: 3.9×10^{-17} $m^2\cdot s^{-1}$ Si face 1473 K: 3.2×10^{-19} $m^2\cdot s^{-1}$ 1773 K: 3.0×10^{-17} $m^2\cdot s^{-1}$	C face 134–197 Si face 372
Costello and Tressler (1986) [62]	Ellipsometry Profilometry	Single crystal (α, green)	O_2, 0.1 MPa	1473–1773	7.2	Parabolic C face 1473 K: 5.8×10^{-18} $m^2\cdot s^{-1}$ 1773 K: 6.4×10^{-17} $m^2\cdot s^{-1}$ Si face 1473 K: 6.8×10^{-19} $m^2\cdot s^{-1}$ 1773 K: 8.3×10^{-17} $m^2\cdot s^{-1}$	C face 121–297 Si face 339
Narushima *et al.* (1989) [63]	Thermogravimetry	CVD (β)	O_2-Ar (P_{O_2}=7 kPa–0.1 MPa)	1823–1948	86.4	Parabolic Stage I (0.1 MPa, amorphous silica) 1823 K: 4.4×10^{-11} $kg^2\cdot m^{-4}\cdot s^{-1}$ 1873 K: 1.1×10^{-10} $kg^2\cdot m^{-4}\cdot s^{-1}$ 1948 K: 2.0×10^{-10} $kg^2\cdot m^{-4}\cdot s^{-1}$ Stage II (0.1 MPa, cristobalite) 1823 K: 1.3×10^{-11} $kg^2\cdot m^{-4}\cdot s^{-1}$ 1873 K: 1.6×10^{-11} $kg^2\cdot m^{-4}\cdot s^{-1}$ 1948 K: 9.7×10^{-11} $kg^2\cdot m^{-4}\cdot s^{-1}$	Stage I: 345 Stage II: 392
Zheng *et al.* (1990) [64]	Ellipsometry	Single crystal (α, 4H)	O_2-Ar (P_{O_2}=100–0.1 MPa)	1473–1773	28.8	Parabolic C face 1473 K: 2.5×10^{-19} $m^2\cdot s^{-1}$ (10^2 Pa) 1473 K: 2.9×10^{-18} $m^2\cdot s^{-1}$ (10^5 Pa) 1773 K: 6.2×10^{-18} $m^2\cdot s^{-1}$ (10^2 Pa) 1773 K: 2.0×10^{-17} $m^2\cdot s^{-1}$ (10^5 Pa) Si face 1473 K: 8.3×10^{-20} $m^2\cdot s^{-1}$ (10^2 Pa) 1473 K: 6.3×10^{-19} $m^2\cdot s^{-1}$ (10^5 Pa) 1773 K: 4.8×10^{-18} $m^2\cdot s^{-1}$ (10^2 Pa) 1773 K: 2.1×10^{-17} $m^2\cdot s^{-1}$ (10^5 Pa)	C face 144–308 (10^2 Pa) 123–220 (10^5 Pa) Si face 298 (10^2 Pa) 240 (10^5 Pa)
Sibieude *et al.* (1991) [65]	XRD	CVD (β)	O_2, 0.1 MPa	1473–1823	90	Linear-parabolic k_p 1583 K: 5.3×10^{-18} $m^2\cdot s^{-1}$ 1748 K: 3.9×10^{-17} $m^2\cdot s^{-1}$ k_l 1583 K: 1.1×10^{-11} $m\cdot s^{-1}$ 1748 K: 1.1×10^{-10} $m\cdot s^{-1}$	k_p: 192 0 k_l: 243
Narushima *et al.* (1993) [66]	Thermogravimetry	CVD (β)	O_2, 0.1 MPa	2003	0.8	Linear 6.3×10^{-6} $kg\cdot m^{-2}\cdot s^{-1}$ (with bubble formation)	

Table 3 Passive oxidation of SiC in wet atmospheres.

Author (year) [Ref. No.]	Method	Type of SiC	Atmosphere	Temperature (K)	Time (ks)	Kinetics	Activation energy ($kJ \cdot mol^{-1}$)
Weaver and Olson (1974) [67]	Thermogravimetry	Hot-pressed	H_2O-Air, 0.1 MPa (P_{H_2O}=2 kPa(?))	1713	24	Parabolic $2.7\times10^{-9}\ kg^2\cdot m^{-4}\cdot s^{-1}$	
Singhal (1976) [68]	Thermogravimetry	Hot-pressed (+MgO)	H_2O-O_2, 0.1 MPa (P_{H_2O}=3.3 kPa)	1523–1623		Parabolic 1523 K: $6.3\times10^{-11}\ kg^2\cdot m^{-4}\cdot s^{-1}$ 1623 K: $1.0\times10^{-9}\ kg^2\cdot m^{-4}\cdot s^{-1}$	527
Suzuki *et al.* (1982) [69]	Ellipsometry	Single crystal (α, 6H)	H_2O-O_2, 0.1 MPa (P_{H_2O}=85 kPa(?))	1123–1373	36	Linear-parabolic k_p 1123 K: $5.6\times10^{-19}\ m^2\cdot s^{-1}$ 1373 K: $2.8\times10^{-17}\ m^2\cdot s^{-1}$ k_l 1123 K: $1.3\times10^{-11}\ m\cdot s^{-1}$ 1373 K: $9.7\times10^{-11}\ m\cdot s^{-1}$	k_p: 201 k_l: 109
Lu *et al.* (1984) [70]	SIMS	Sputtered	H_2O-O_2, 0.1 MPa (P_{H_2O}=85 kPa(?))	1173–1373	57.6	Linear 1173 K: $2.5\times10^{-12}\ m\cdot s^{-1}$ 1373 K: $3.3\times10^{-11}\ m\cdot s^{-1}$	209
Fung and Kopanski (1984) [71]	Ellipsometry	CVD (β)	H_2O-O_2, 0.1 MPa (P_{H_2O}=85 kPa(?))	1273–1523	180	Linear-parabolic k_p 1373 K: $1.8\times10^{-17}\ m^2\cdot s^{-1}$ 1523 K: $1.2\times10^{-16}\ m^2\cdot s^{-1}$ k_l 1373 K: $6.9\times10^{-12}\ m\cdot s^{-1}$ 1523 K: $9.2\times10^{-11}\ m\cdot s^{-1}$	k_p: 209 k_l: 310
Tressler *et al.* (1985) [72]	Ellipsometry	Single crystal (α, black)	Steam, 0.1 MPa H_2O-O_2, 0.1 MPa (P_{H_2O}=3.3 kPa)	1473–1773		Parabolic Steam 1473 K: $1.2\times10^{-16}\ m^2\cdot s^{-1}$ 1723 K: $5.0\times10^{-16}\ m^2\cdot s^{-1}$ H_2O-O_2 1473 K: $8.2\times10^{-18}\ m^2\cdot s^{-1}$ 1773 K: $6.1\times10^{-17}\ m^2\cdot s^{-1}$	k_p: 118 k_p: 145
Tressler *et al.* (1985) [72]	Ellipsometry	PLS (α) (+B)	Steam, 0.1 MPa H_2O-O_2, 0.1 MPa (P_{H_2O}=3.3 kPa)	1473–1773		Parabolic Steam 1473 K: $3.0\times10^{-17}\ m^2\cdot s^{-1}$ 1723 K: $2.7\times10^{-16}\ m^2\cdot s^{-1}$ H_2O-O_2 1473 K: $6.7\times10^{-18}\ m^2\cdot s^{-1}$ 1773 K: $5.0\times10^{-17}\ m^2\cdot s^{-1}$	k_p: 186 k_l: 145
Maeda *et al.* (1988) [73]	Gravimetry	PLS (+Al_2O_3)	H_2O-Air, 0.1 MPa (P_{H_2O}=10–40 kPa)	1573	1296	Parabolic P_{H_2O}=10 kPa: $1.0\times10^{-10}\ kg^2\cdot m^{-4}\cdot s^{-1}$ P_{H_2O}=20 kPa: $6.9\times10^{-11}\ kg^2\cdot m^{-4}\cdot s^{-1}$ P_{H_2O}=30 kPa: $7.8\times10^{-11}\ kg^2\cdot m^{-4}\cdot s^{-1}$ P_{H_2O}=40 kPa: $9.3\times10^{-11}\ kg^2\cdot m^{-4}\cdot s^{-1}$	
Narushima *et al.* (1990) [74]	Thermogravimetry	CVD (β)	H_2O-O_2, 0.1 MPa (P_{H_2O}=10 kPa)	1823–1923	86.4	Linear-parabolic k_p 1823 K: $3.2\times10^{-10}\ kg^2\cdot m^{-4}\cdot s^{-1}$ 1923 K: $1.1\times10^{-9}\ kg^2\cdot m^{-4}\cdot s^{-1}$ k_l 1823 K: $1.6\times10^{-8}\ kg\cdot m^{-2}\cdot s^{-1}$ 1923 K: $7.6\times10^{-8}\ kg\cdot m^{-2}\cdot s^{-1}$	k_p: 397 k_l: 428
Opila (1994) [75]	Thermogravimetry	CVD	H_2O-O_2, 0.1 MPa (P_{H_2O}=10 kPa)	1473–1673	396	Parabolic 1473 K: $4.4\times10^{-12}\ kg^2\cdot m^{-4}\cdot s^{-1}$ 1673 K: $1.8\times10^{-11}\ kg^2\cdot m^{-4}\cdot s^{-1}$	41

has a maximum value around 1950 K[95], and the amorphous phase is dominant at the temperatures below 1573 K and around the melting point of cristobalite. The oxidation rates with cristobalite film are lower than those with amorphous SiO_2 film[63]. The cristobalite films are not appropriate for cyclic oxidation because cracks with spherulitic features are caused by volume contraction (6%) due to the transformation[96] of β-cristobalite to α-cristobalite during the cooling process[63][97]–[99].

The possible rate-controlling step of the passive oxidation is oxygen diffusion inward, CO diffusion outward and/or an interfacial reaction[42]. Since the parabolic oxidation is observed for highly pure and dense SiC, the rate-controlling step may be due to the diffusion of chemical species in the oxide film. However, the diffusion species are not clarified up to now. Luthra[100] examined the data so far reported on the oxidation of SiC and concluded that both of diffusion and the interfacial reaction were rate controlling (mixed control mechanism).

The formation of SiO_2 bubbles can be closely related to the oxidation mechanism of SiC, and is important for a practical use whether bubbles are formed or not be-

Table 4 Active oxidation of SiC.

Author (year) [Ref. No.]	Method	Type of SiC	Atmosphere	Temperature (K)	Kinetics	Transition
Gulbransen *et al.* (1966) [58]	Thermogravimetry	Single crystal (α, 6H)	O_2 (P_{total}=1.2–66 Pa)	1473–1673	Linear 1523 K: 9.4×10^{-6} kg·m^{-2}·s^{-1} (P_{total}=1.2 Pa) 1673 K: 4.7×10^{-4} kg·m^{-2}·s^{-1} (P_{total}=13 Pa)	$P^t_{O_2}$ 1473 K: 1.3 Pa 1673 K: 66 Pa
Rosner and Allendorf (1970) [76]	Gravimetry	CVD (β)	O_2, O, N_2, N (P_{total}>0.01 Pa)	1750–2400	Linear?	$P^t_{O_2}$ 1800 K: 1.3 Pa 2000 K: 13 Pa P^t_O 1870 K: 0.07 Pa 2000 K: 2.6 Pa
Antill and Warburton (1971) [77]	Thermogravimetry	CVD (β)	O_2, CO_2, H_2O (P_{total}<10 Pa)	1273–1473	Linear	$P^t_{O_2}$ 1000 K: <0.4 Pa $P^t_{CO_2}$ 1000 K: <0.4 Pa 1200 K: 1–20 Pa $P^t_{H_2O}$ 1000 K: 0.4 Pa 1200 K: 3–10 Pa
Elchin *et al.* (1971) [78]	Gravimetry	PLS, 93%SiC (+5.5Si+0.5C)	Air, CO_2, Steam (P_{total}=0.1 MPa)	2370, 2720	Linear Air 2370 K: 6.5×10^{-3} kg·m^{-2}·s^{-1} 2720 K: 1.6×10^{-2} kg·m^{-2}·s^{-1} CO_2 2370 K: 1.0×10^{-2} kg·m^{-2}·s^{-1} 2720 K: 1.2×10^{-2} kg·m^{-2}·s^{-1} Steam 2370 K: 3.1×10^{-2} kg·m^{-2}·s^{-1} 2720 K: 3.8×10^{-2} kg·m^{-2}·s^{-1}	
Bennett and Chaffey (1974) [79]	Gravimetry	Reaction sintered (+16%Si)	Xe-O_2 (CuO/Cu_2O) (P_{total}=26 kPa)	1223	Linear $1.7\text{–}4.2\times10^{-10}$ kg·m^{-2}·s^{-1}	$P^t_{O_2}$ <0.09 Pa
Hinze and Graham (1976) [80]	Thermogravimetry	Hot-pressed (β) (+0.15%B +0.05%W)	Ar-O_2 (P_{total}=20 kPa) ($V=1.4\times10^{-6}$ m^3·s^{-1})	1643–1803	Linear 1750 K: 1.0×10^{-5} kg·m^{-2}·s^{-1} (P_{O_2}=40 kPa)	$P^t_{O_2}$ 1653 K: 7.1 Pa 1803 K: 158 Pa
Kim and Readey (1989) [81]	Thermogravimetry	PLS (α) (+0.5%C +0.5%B)	H_2-H_2O (P_{total}=0.1 MPa) (P_{H_2O}=2–500 Pa) ($V=2.7\times10^{-3}$–1.7×10^{-2} m·s^{-1})	1673–1800	Linear 1673 K, 5.9×10^{-3} m·s^{-1} 8×10^{-7} kg·m^{-2}·s^{-1} (P_{H_2O}=2 Pa) 8×10^{-7} kg·m^{-2}·s^{-1} (P_{H_2O}=50 Pa) 5×10^{-7} kg·m^{-2}·s^{-1} (P_{H_2O}=500 Pa) 1800 K, 5.9×10^{-3} m·s^{-1} 3×10^{-6} kg·m^{-2}·s^{-1} (P_{H_2O}=2 Pa) 6×10^{-5} kg·m^{-2}·s^{-1} (P_{H_2O}=50 Pa) 6×10^{-6} kg·m^{-2}·s^{-1} (P_{H_2O}=500 Pa)	
Vaughn and Maahs (1990) [82]	Thermogravimetry	PLS (α) (+C+B)	Air (P_{O_2}=2.5–123 kPa) ($V=1.7\times10^{-7}$–1.7×10^{-6} m^3·s^{-1})	1620–1816		$P^t_{O_2}$ 1620 K: 2.5 Pa (1.7×10^{-7} m^3·s^{-1}) 1816 K: 123 Pa (8.3×10^{-7} m^3·s^{-1})
Kim and Moorhead (1990) [44]	Gravimetry	PLS (α) (+C+B)	Ar-O_2 (P_{total}=0.1 MPa) (P_{O_2}=0.75–150 Pa)	1673	Linear 3.1×10^{-7} kg·m^{-2}·s^{-1} (P_{O_2}=15 Pa)	$P^t_{O_2}$ 20–30 Pa
Jacobson *et al.* (1990) [83]	Thermogravimetry	PLS (α) (+B)	Ar-5%H_2 ($P_{O_2}=10^{-17}$ Pa) ($V=5.3\times10^{-3}$–2.1×10^{-2} m·s^{-1})	1573	Linear 1.4×10^{-7} kg·m^{-2}·s^{-1} ($V=5.3\times10^{-3}$ m·s^{-1}) 2.5×10^{-7} kg·m^{-2}·s^{-1} ($V=2.1\times10^{-2}$ m·s^{-1})	
Butt *et al.* (1991) [84]	Gravimetry	PLS (+B) (+Al)	N_2-1.2%H_2-0.6%CO (P_{total}=130 Pa)	1573	Linear (?) 5.6×10^{-9} kg·m^{-2}·s^{-1} (B doped) 8.3×10^{-9} kg·m^{-2}·s^{-1} (Al doped)	
Narushima *et al.* (1991) [55]	Thermogravimetry	CVD (β)	Ar-O_2 (P_{total}=0.1 MPa) (P_{O_2}=6–500 Pa) ($V=0.41\text{–}3.7\times10^{-2}$ m·s^{-1})	1840–1923	Linear 1923 K, 1.3×10^{-2} m·s^{-1} 2.0×10^{-5} kg·m^{-2}·s^{-1} (P_{O_2}=10 Pa) 5.8×10^{-5} kg·m^{-2}·s^{-1} (P_{O_2}=30 Pa)	$P^t_{O_2}$ 1848 K: 95 Pa (1.3×10^{-2} m·s^{-1}) 1923 K: 330 Pa (1.3×10^{-2} m·s^{-1})

Table 4 Continued.

Balat *et al.* (1992) [85]	Gravimetry	PLS (α) ($+$B)	Air (P_{O_2}=200-2100 Pa) ($V=1.1\times10^{-6}$ m$^3\cdot$s^{-1})	1673-1973		$P^t_{O_2}$ 1770 K: 1500 Pa P^t_O 1840 K: 1000 Pa
Butt *et al.* (1992) [86]	Thermogravimetry	Reaction sintered (α, $+$Si) PLS (α, $+$B) (α, $+$Al)	Endothermic gas (38%N_2-41%H_2-21%CO) (P_{total}=133 Pa) Nitrogen-based gas (N_2-1.2%H_2-0.6%CO) (P_{total}=133 Pa)	1373-1623	Linear PLS (B doped) Nitrogen-based gas 1373 K: 1.1×10^{-9} kg$\cdot$m$^{-2}\cdot$s^{-1} 1623 K: 6.9×10^{-9} kg$\cdot$m$^{-2}\cdot$s^{-1} Reaction sintered Endothermic gas 1573 K: 1.1×10^{-7} kg$\cdot$m$^{-2}\cdot$s^{-1}	
Narushima *et al.* (1993) [87]	Thermogravimetry	CVD (β)	CO-CO_2 (P_{total}=0.1 MPa) ($P_{CO_2}/P_{CO}=10^{-4}$-10^{-1}) (V=0.486-14.6$\times10^{-2}$ m$^3\cdot$s^{-1})	1823-1923	Linear 1923 K, 1.95×10^{-2} m$\cdot$s^{-1} 2.5×10^{-7} kg$\cdot$m$^{-2}\cdot$s^{-1} ($P_{CO_2}/P_{CO}=10^{-4}$) 6.3×10^{-6} kg$\cdot$m$^{-2}\cdot$s^{-1} ($P_{CO_2}/P_{CO}=10^{-3}$) 4.0×10^{-6} kg$\cdot$m$^{-2}\cdot$s^{-1} ($P_{CO_2}/P_{CO}=10^{-2}$)	
Narushima *et al.* (1994) [88]	Thermogravimetry	CVD (β)	CO-CO_2 (P_{total}=0.1 MPa) ($P_{CO_2}/P_{CO}=10^{-1}$-10^{1}) ($V=1.95\times10^{-2}$ m$\cdot$s^{-1})	1823-1923	Linear 1823 K, 1.95×10^{-2} m$\cdot$s^{-1} 1.5×10^{-8} kg$\cdot$m$^{-2}\cdot$s^{-1} ($P_{CO_2}/P_{CO}=10^{0}$)	$(P_{CO_2}/P_{CO})^t$ 1873 K: $10^{0.5}$-10^{1}

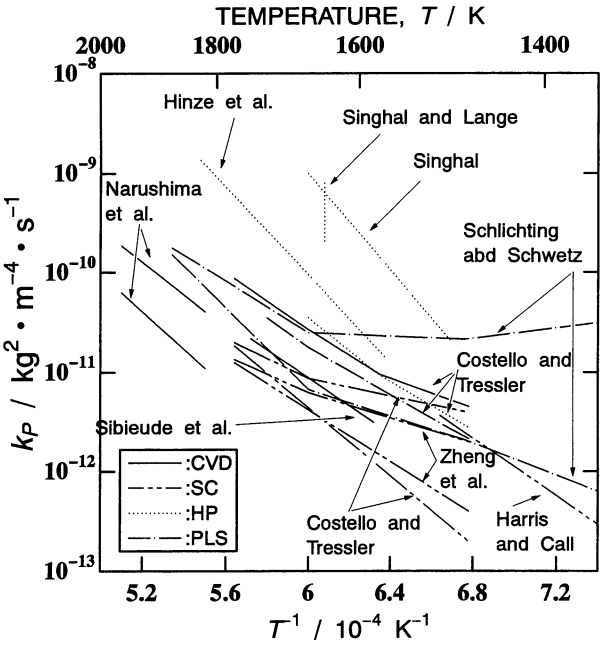

Fig. 6 Comparison of the parabolic rate constants of SiC in dry oxygen.

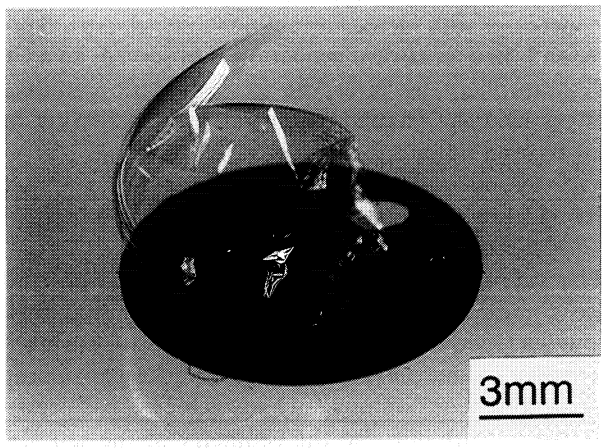

Fig. 7 Optical micrograph of CVD-SiC oxidized at 1923 K in a CO-CO_2 atmosphere.

cause bubble formation means that the SiO_2 film is no longer protective to further oxidation. Figure 7 shows the optical micrograph of an SiO_2 bubble formed on CVD-SiC at 1923 K in a CO-CO_2 atmosphere. The SiO_2 film was not protective in this condition. The bubble formation is observed above 1950 K in an oxygen atmosphere[66][101], while above 1900 K in a CO-CO_2 atmosphere[88]. The bubble formation means that CO gas should be accumulated at the SiC/SiO_2 interface. These results suggest that the inward diffusion of oxygen or CO_2 through the SiO_2 films may be faster than the outward diffusion of CO, and the rate-controlling step depends on the atmosphere and temperature.

It is well-known that water vapor accelerates the oxidation of SiC[38][39]. Parabolic, linear and linear-parabolic kinetics have been reported for wet oxidation of SiC as shown in Table 3. Water vapor extends the linear kinetic region and increases the parabolic rate constant[74]. Activation energy of wet oxidation in the parabolic kinetic region is higher than that of the diffusion of water vapor in amorphous SiO_2 (75 kJ$\cdot$mol^{-1})[102][103], and the rate-controlling step was reported to be diffusion of oxygen[74] or CO gas[69][71]. The dissolution reaction of water vapor in SiO_2 can be represented by eq. (10)[104].

$$(O^0)+H_2O(g)=2(OH) \quad (10)$$

where (O^0) and (OH) are bridging oxygen and hydroxyl group in SiO_2, respectively. The solubility of OH in SiO_2 was reported to be 700 ppm (1473 K, 92 kPa water vapor)[102], which was a few order of magnitude larger than that of oxygen[105]. It has been reported[106]-[108] that water vapor modified the microstructure of SiO_2 and led to the decrease of viscosity and density, the increase of expansion coefficient and crystallization of amorphous

SiO_2. The modification of the oxide film means that the diffusion of chemical species through it in wet oxidation is faster than that in dry oxidation. Therefore, it is speculated that the difference of microstructure of the SiO_2 film between wet and dry oxidation influences the oxidation rates. Further studies on the physical and thermodynamic properties of SiO_2 and systematic oxidation experiments are needed in order to understand the wet oxidation mechanism.

2. Active oxidation

Three kinds of atmospheres are employed for the experimental study of active oxidation as follows;

(a) low total gas pressure (P_{total}=1–1000 Pa)[58][76][77][82][85]
(b) inert gas-oxygen mixture gas[55][79][80]
(c) CO–CO_2 or H_2–H_2O mixture gas[44][81][83][87][88]

Figure 8 illustrates the difference of the active oxidation behavior between in an inert gas-oxygen mixture gas[55] and in a CO–CO_2 or an H_2–H_2O mixture gas[87] for SiC. In an inert gas-oxygen atmosphere, the active oxidation rate increases with increasing ambient oxygen partial pressure, and then an abrupt transition is observed. In a CO–CO_2 atmosphere, however, the active oxidation gradually changes into the passive oxidation with increasing ambient oxygen potential.

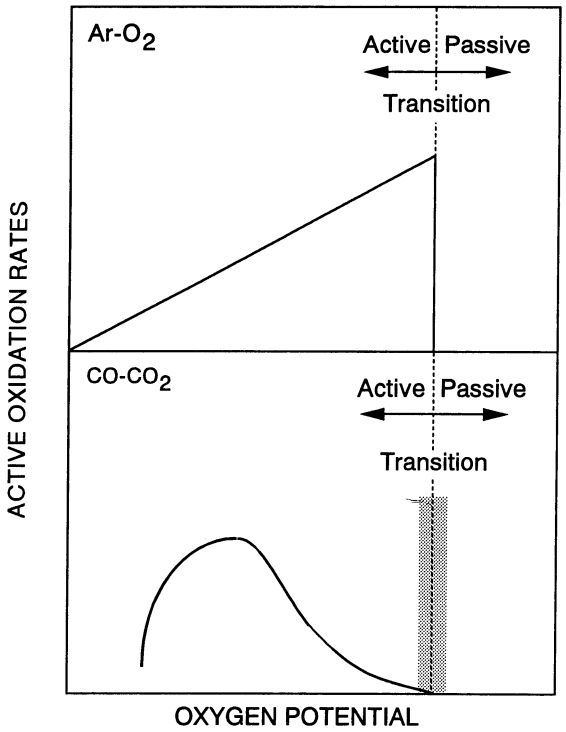

Fig. 8 Schematic diagram of active-to-passive transition in Ar–O_2 and CO–CO_2 atmospheres.

(1) In low total gas pressure or inert gas-oxygen mixture gas

The rate-controlling step of active oxidation under these conditions is considered to be oxygen diffusion through a gaseous boundary layer near the SiC surface[55]. The active oxidation rate in Table 5 varies considerably because it depends on not only gas velocity, gas pressure and temperature but also the geometry of the sample.

Figure 9 summarizes the $P^t_{O_2}$ values of SiC reported so far. $P^t_{O_2}(I)$ and $P^t_{O_2}(W)$ in Fig. 9 are the $P^t_{O_2}$ values calculated from volatility diagram and Wagner model, respectively. All the experimental values of $P^t_{O_2}$ are between $P^t_{O_2}(I)$ and $P^t_{O_2}(W)$. The $P^t_{O_2}$ values are within two orders of magnitude except those of Rosner and Allendorf[76] who examined a chemical reaction limited active oxidation behavior free from the effects of diffusion phenomena. These results suggest that the volatility diagram and Wagner model are appropriate to explain the active-to-passive transition for SiC. The formation of SiO_2 smoke (eq. (9)) may cause the lower $P^t_{O_2}$ values than the $P^t_{O_2}(W)$ values.

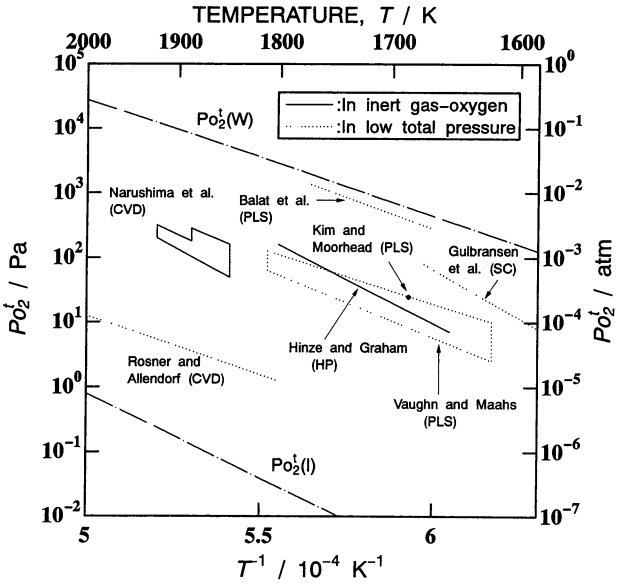

Fig. 9 Comparison of the active-to-passive transition oxygen partial pressure of SiC.

(2) In CO–CO_2 or H_2–H_2O atmosphere

The chemical equilibrium of a CO–CO_2 or an H_2–H_2O mixture gas is suitable to produce lower oxygen potentials. Active oxidation behavior of SiC in a CO–CO_2 and an H_2–H_2O atmosphere has been investigated by the present authors[87][88] and Kim and Ready[81], respectively. The effects of oxygen potential, temperature and gas velocity on the active oxidation rate were reported. The active oxidation rate shows maxima at a certain value of P_{CO_2}/P_{CO} or P_{H_2O}/P_{H_2}. In an oxygen potential region higher than the maxima, a discontinuous SiO_2 layer is formed on the SiC surface by the reaction of SiC with the oxidant (CO_2 in CO–CO_2 or H_2O in H_2–H_2O) and the SiO gas is formed by the reaction of the discontinuous SiO_2 with reductant (CO in CO–CO_2 or H_2 in H_2–H_2O). The reactions of formation of SiO_2 and SiO in a CO–CO_2 atmosphere are represented by eqs. (11) and (12), respectively.

$$SiC(s)+3CO_2(g)=SiO_2(s)+4CO(g) \quad (11)$$

$$SiO_2(s)+CO(g)=SiO(g)+CO_2(g) \quad (12)$$

The diffusion of gas species formed by the reduction of SiO_2 may control the active oxidation rates[88]. In an oxygen potential region lower than maxima, the active oxidation mechanism in a CO–CO_2 atmosphere is different from that in an H_2–H_2O atmosphere. The formation of carbon was observed on SiC surface in CO–CO_2 atmospheres ($P_{CO_2}/P_{CO}<10^{-2.5}$), and the CO_2 diffusion to the SiC surface might be rate controlling (1823–1923 K)[87]. The rate-controlling step of the active oxidation in an H_2–H_2O atmosphere was reported to be gaseous diffusion through a gaseous boundary layer above 1700 K and chemical reaction on the SiC surface below 1673 K[81].

A few reports have dealt with the transition and the active-to-passive transition of SiC in a CO–CO_2 or an H_2–H_2O atmosphere. The present authors defined the transition P_{CO_2}/P_{CO} as a critical P_{CO_2}/P_{CO} value at which the mass change is neither loss nor gain, and reported that the transition was observed around $P_{CO_2}/P_{CO}=10^{0.5}$–10^{1} in CO–CO_2 atmospheres using a thermogravimetric technique[88]. The experimental transition P_{CO_2}/P_{CO} value was found to be two orders of magnitude larger than the value calculated from Wagner model, in which the effect of mass loss by the CO reduction of SiO_2 (eq. (12)) is not included.

IV. Oxidation of Si_3N_4

1. Passive oxidation

The studies on passive oxidation in dry and wet

Table 5 Passive oxidation of Si_3N_4 in dry atmospheres.

Author (year) [Ref. No.]	Method	Type of Si_3N_4	Atmosphere	Temperature (K)	Time (ks)	Kinetics	Activation energy ($kJ\cdot mol^{-1}$)
Fränz and Langheinrich (1971) [109]	Interferometry	CVD (amorphous)	O_2, 0.1 MPa	1273–1533	86.4	Parabolic 1503 K: $1.8\times10^{-19}\ m^2\cdot s^{-1}$ 1533 K: $3.2\times10^{-19}\ m^2\cdot s^{-1}$	
Rosolowski and Greskovich (1974) [110]		CVD (α)	Air, 0.1 MPa	1683–1823		Parabolic 1683 K: $1.1\times10^{-11}\ kg^2\cdot m^{-4}\cdot s^{-1}$ 1823 K: $6.4\times10^{-12}\ kg^2\cdot m^{-4}\cdot s^{-1}$	
Mellottee *et al.* (1976) [111]	Thermogravimetry	CVD (amorphous)	O_2, 0.1 MPa	1573		Parabolic 5.3×10^{-11}–$3.3\times10^{-10}\ kg^2\cdot m^{-4}\cdot s^{-1}$	
Enomoto *et al.* (1978) [112]	Ellipsometry Interferometry	CVD	O_2, 0.1 MPa	1373	79.2	$X=k_e\cdot t^{2/3}$ k_e: $1.0\times10^{-10}\ m\cdot min^{-2/3}$	
Galasso *et al.* (1978) [113]	Thermogravimetry	CVD (α)	Air, 0.1 MPa	1623	234	Parabolic(?) $6.8\times10^{-11}\ kg^2\cdot m^{-4}\cdot s^{-1}$	
Hirai *et al.* (1980) [114]	Thermogravimetry	CVD (amorphous)	O_2, 0.1 MPa	1823–1923	36	Parabolic (<1923 K) 1823 K: $1.5\times10^{-11}\ kg^2\cdot m^{-4}\cdot s^{-1}$ 1903 K: $5.8\times10^{-11}\ kg^2\cdot m^{-4}\cdot s^{-1}$ Linear (1923 K) $1.6\times10^{-7}\ kg\cdot m^{-2}\cdot s^{-1}$	k_p: 460
Hirai *et al.* (1980) [114]	Thermogravimetry	CVD (α)	O_2, Air, 0.1 MPa	1823–1923	36	Parabolic O_2 1823 K: $5.8\times10^{-11}\ kg^2\cdot m^{-4}\cdot s^{-1}$ 1923 K: $2.2\times10^{-10}\ kg^2\cdot m^{-4}\cdot s^{-1}$ Air 1823 K: $3.6\times10^{-12}\ kg^2\cdot m^{-4}\cdot s^{-1}$	O_2: 390
Chramova *et al.* (1981) [115]	Ellipsometry Interferometry	CVD (amorphous)	O_2, 0.1 MPa	1273–1373	24	Linear-parabolic k_p 1273 K: $1.1\times10^{-20}\ m^2\cdot s^{-1}$ 1373 K: $5.0\times10^{-20}\ m^2\cdot s^{-1}$ k_l 1373 K: 9–$19.5\times10^{-10}\ m\cdot s^{-1}$	k_p: 218
Du *et al.* (1989) [116]	Ellipsometry	CVD (α)	O_2–N_2–Ar, 0.1 MPa (P_{O_2}=5 kPa–0.1 MPa)	1373–1673	28.8	Parabolic O_2 (0.1 MPa) 1373 K: $5.0\times10^{-21}\ m^2\cdot s^{-1}$ 1673 K: $1.1\times10^{-17}\ m^2\cdot s^{-1}$ O_2–Ar (P_{O_2}=5 kPa) 1673 K: $5.7\times10^{-18}\ m^2\cdot s^{-1}$	481
Choi *et al.* (1989) [117]	Ellipsometry	CVD (α)	O_2, 0.1 MPa	1307–1573		Parabolic $9.1\times10^{-8}\exp(-39700/T)\ m^2\cdot s^{-1}$	330
Narushima *et al.* (1993) [66]	Thermogravimetry	CVD (α)	O_2, 0.1 MPa	1923–2003	36	Parabolic 1923 K: $1.3\times10^{-10}\ kg^2\cdot m^{-4}\cdot s^{-1}$ 1953 K: $3.0\times10^{-10}\ kg^2\cdot m^{-4}\cdot s^{-1}$ 1973 K: $1.4\times10^{-9}\ kg^2\cdot m^{-4}\cdot s^{-1}$ Linear 2003 K: $4.0\times10^{-7}\ kg\cdot m^{-2}\cdot s^{-1}$	

atmospheres and active oxidation of Si_3N_4 are summarized in Tables 5[66][109]-[117], 6[68][109][112][117]-[124] and 7[45][56][57][82][118][125]-[128], respectively. The data on the highly dense and pure sample, CVD-Si_3N_4, are shown in Table 5. The parabolic rate constants (k_p) of CVD-Si_3N_4 are compared with those of HP-Si_3N_4[125][129][130] in Fig. 10. The k_p values for dry oxidation of CVD-Si_3N_4 with good agreement are obtained. The k_p values of HP-Si_3N_4 are much larger than those of CVD-Si_3N_4. It is suggested that a sintering additive, such as MgO or Y_2O_3 in a HP-Si_3N_4 body plays an important role in the oxidation process. The silicate glasses in the SiO_2–MgO or SiO_2–Y_2O_3 system will be formed as oxidation products[130]-[132] on HP-Si_3N_4 even below the eutectic point of these systems[133]. Since Mg^{2+} or Y^{3+} may act as a network modifier[134] in the silicate glasses, the diffusion rates of chemical species in the silicate glass films are larger than those in pure silica. Therefore, the oxidation rates of Si_3N_4 containing

Table 6 Passive oxidation of Si_3N_4 in wet atmospheres.

Author (year) [Ref. No.]	Method	Type of Si_3N_4	Atmosphere	Temperature (K)	Time (ks)	Kinetics	Activation energy ($kJ \cdot mol^{-1}$)
Fränz and Langheinrich (1971) [109]	Interferometry	CVD (amorphous)	H_2O-O_2, 0.1 MPa (P_{H_2O}=85 kPa(?))	1073-1373	72	Parabolic 1373 K: 3.8×10^{-19} $m^2\cdot s^{-1}$	
Singhal (1976) [68]	Thermogravimetry	Hot-pressed (+MgO)	H_2O-O_2, 0.1 MPa (P_{H_2O}=3.3 kPa)	1473-1623		Parabolic 1473 K: 2.5×10^{-11} $kg^2\cdot m^{-4}\cdot s^{-1}$ 1623 K: 1.6×10^{-9} $kg^2\cdot m^{-4}\cdot s^{-1}$	488
Warburton *et al.* (1978) [118]	Gravimetry	Reaction sintered	H_2O-Air, 0.1 MPa (P_{H_2O}=2.5 kPa)	973-1373	28800	%Conversion, 18000 ks 1273 K: 70% 1373 K: 21% (density of Si_3N_4=2.31×10^3 $kg\cdot m^{-3}$)	
Enomoto *et al.* (1978) [112]	Ellipsometry Interferometry	CVD	H_2-O_2, 0.1 MPa (P_{H_2O}=25-95 kPa)	1173-1373	111.6	$X=k_e\cdot t^{2/3}$ 1173 K: 1.0×10^{-10} $m\cdot min^{-2/3}$ 1373 K: 1.1×10^{-9} $m\cdot min^{-2/3}$	161
Hui *et al.* (1982) [119]	Ellipsometry	Implanted Nitridation of Si	H_2O-O_2, 0.1 MPa	1173-1373	11.4	Linear Implanted 1173 K: 2.8×10^{-13} $m\cdot s^{-1}$ 1373 K: 5.6×10^{-12} $m\cdot s^{-1}$	198
Sato *et al.* (1987) [120]	Gravimetry	Hot-pressed (+1%Al+3.7%Y) PLS (+3.6%Al+3.5%Y)	H_2O-N_2, 0.1 MPa (P_{H_2O}=1.5-20 kPa)	1373-1623	234	Parabolic PLS 1523 K: 1.9×10^{-9} $kg^2\cdot m^{-4}\cdot s^{-1}$ (P_{H_2O}=25-95 kPa)	PLS 809
Kuiper *et al.* (1989) [121]	Gravimetry	CVD	H_2-O_2, 0.1 MPa (P_{H_2O}=25-90 kPa)	1123-1273	57.6	Linear 1123 K: 1.1×10^{15} $Oatoms\cdot m^{-2}\cdot s^{-1}$ 1273 K: 1.4×10^{16} $Oatoms\cdot m^{-2}\cdot s^{-1}$ (P_{H_2O}=90 kPa)	192
Choi *et al.* (1989) [117]	Gravimetry	CVD (α)	H_2O-O_2(-He, Ar), 0.1 MPa (P_{H_2O}=4 kPa-0.1 MPa)	1315-1564		Parabolic H_2O-O_2 (P_{H_2O}=4 kPa) $1.0\times10^{-6}\exp(-41450/T)$ $m^2\cdot s^{-1}$ H_2O (P_{H_2O}=101 kPa) $1.4\times10^{-10}\exp(-31190/T)$ $m^2\cdot s^{-1}$ H_2O-Ar (P_{H_2O}=51 kPa) $2.2\times10^{-8}\exp(-38110/T)$ $m^2\cdot s^{-1}$ H_2O-He (P_{H_2O}=51 kPa) $8.0\times10^{-8}\exp(-40170/T)$ $m^2\cdot s^{-1}$	259-350
Maeda *et al.* (1990) [122]	Gravimetry	Hot-pressed (+0.15%Al+0.20%Cr +1.4%Sc) (+0.98%Al+2.9%Y) (+1.29%Al+3.8%Y) PLS (+1.8%Al+0.73%Y) (+1.2%Al+3.3%Y)	H_2O-Air, 0.1 MPa (P_{H_2O}=1-40 kPa)	1573	360	Parabolic(?) PLS (+1.2%Al+3.3%Y) $2.3\text{-}9.0\times10^{-10}$ $kg^2\cdot m^{-4}\cdot s^{-1}$ (P_{H_2O}=1-40 kPa) Hot-pressed (+1.29%Al+3.8%Y) $4.4\text{-}6.9\times10^{-11}$ $kg^2\cdot m^{-4}\cdot s^{-1}$ (P_{H_2O}=1-40 kPa)	
Fourrier *et al.* (1991) [123]	Ellipsometry	Sputtered CVD	H_2O-O_2, 0.1 MPa (P_{H_2O}>80 kPa)	1173-1373	36	Linear-parabolic (Si_3N_4 consumed) k_p 1273 K: 5.7×10^{-20} $m^2\cdot s^{-1}$ k_l 1273 K: 4.5×10^{-8} $m\cdot s^{-1}$	
Narushima *et al.* (1994) [124]	Thermogravimetry	CVD (α)	H_2O-O_2, 0.1 MPa (P_{H_2O}=6, 10 kPa)	1573-1923	86.4	Linear P_{H_2O}=10 kPa 1573 K: 1.4×10^{-8} $kg^2\cdot m^{-4}\cdot s^{-1}$ 1773 K: 1.2×10^{-8} $kg^2\cdot m^{-4}\cdot s^{-1}$ 1923 K: 9.3×10^{-8} $kg^2\cdot m^{-4}\cdot s^{-1}$	

Table 7 Active oxidation of Si_3N_4.

Author (year) [Ref. No.]	Method	Type of Si_3N_4	Atmosphere	Temperature (K)	Kinetics	Transition
Tripp and Graham (1976) [125]	Thermogravimetry	Hot-pressed (+MgO)	CO-CO_2 (P_{total}=20 kPa) ($V=1.3\times10^{-6}$ m$^3\cdot$s^{-1})	1673		$P^t_{O_2}$ 10^{-2}-10^{-4} Pa
Warburton *et al.* (1978) [118]	Gravimetry	Reaction sintered	Air ($P_{total}=0.3\text{-}3\times10^{-2}$ Pa)	1323-1473	Linear 1323 K: 7.0×10^{-10} kg$\cdot$m$^{-2}\cdot$s^{-1} 1473 K: 7.0×10^{-8} kg$\cdot$m$^{-2}\cdot$s^{-1}	P^t_{air} 1323 K: 0.05 Pa 1473 K: 2 Pa
Sheehan (1982) [126]	Gravimetry	Hot-pressed (+1%MgO) (+5%MgO)	He-O_2 (P_{total}=0.15 MPa) (P_{O_2}=0.4-0.8 Pa)	1273-1473		1%MgO: 1373-1473 K 5%MgO: 1273-1373 K ($P^t_{O_2}$=0.4-0.8 Pa)
Kim (1987) [127]	Thermogravimetry	CVD (α)	H_2-H_2O (P_{total}=0.1 MPa) (P_{H_2O}=2-7000 Pa) ($V=0.2\text{-}3\times10^{-2}$ m$\cdot$s^{-1})	1573-1800	Linear 1600 K, 5.9×10^{-3} m$\cdot$s^{-1} 2.5×10^{-7} kg$\cdot$m$^{-2}\cdot$s^{-1} (P_{H_2O}=10 Pa) 1.0×10^{-7} kg$\cdot$m$^{-2}\cdot$s^{-1} (P_{H_2O}=100 Pa) 6.3×10^{-8} kg$\cdot$m$^{-2}\cdot$s^{-1} (P_{H_2O}=1000 Pa) 1800 K, 5.9×10^{-3} m$\cdot$s^{-1} 1.0×10^{-5} kg$\cdot$m$^{-2}\cdot$s^{-1} (P_{H_2O}=10 Pa) 1.6×10^{-5} kg$\cdot$m$^{-2}\cdot$s^{-1} (P_{H_2O}=100 Pa) 7.9×10^{-6} kg$\cdot$m$^{-2}\cdot$s^{-1} (P_{H_2O}=1000 Pa)	
Kim (1987) [127]	Thermogravimetry	Hot-pressed (+6%Y_2O_3+MgO)	H_2-H_2O (P_{total}=0.1 MPa) (P_{H_2O}=2-7000 Pa) ($V=5.9\times10^{-3}$ m$\cdot$s^{-1})	1573-1723	Linear 1600 K, 5.9×10^{-3} m$\cdot$s^{-1} 2.5×10^{-6} kg$\cdot$m$^{-2}\cdot$s^{-1} (P_{H_2O}=10 Pa) 1723 K, 5.9×10^{-3} m$\cdot$s^{-1} 2.0×10^{-5} kg$\cdot$m$^{-2}\cdot$s^{-1} (P_{H_2O}=10 Pa) 5.0×10^{-6} kg$\cdot$m$^{-2}\cdot$s^{-1} (P_{H_2O}=100 Pa)	
Du (1988) [128]	Ellipsometry	CVD (α)	Ar-O_2 (P_{total}=0.1 MPa)	1473-1673		$P^t_{O_2}$ 0.1 Pa
Vaughn and Maahs (1990) [82]	Thermogravimetry	Hot-pressed (+MgO)	Air (P_{O_2}=7.1-206 Pa) ($V=5.6\times10^{-7}$ m$^3\cdot$s^{-1})	1639-1793		$P^t_{O_2}$ 1639 K: 7.1 Pa 1793 K: 206 Pa
Vaughn and Maahs (1990) [82]	Thermogravimetry	PLS (+6%Y_2O_3)	Air (P_{O_2}=7.0-111.0 Pa) ($V=5.6\times10^{-7}$ m$^3\cdot$s^{-1})	1638-1753		$P^t_{O_2}$ 1638 K: 7.0 Pa 1753 K: 111 Pa
Kim and Moorhead (1990) [45]	Gravimetry	CVD	H_2-H_2O (P_{total}=0.1 MPa) ($V=9\times10^{-3}$ m$\cdot$s^{-1}) Ar-O_2 (P_{total}=0.1 MPa) ($V=9\times10^{-3}$ m$\cdot$s^{-1})	1673	Linear H_2-H_2O 3×10^{-7} kg$\cdot$m$^{-2}\cdot$s^{-1} (P_{H_2O}=1-100 Pa)	$P^t_{O_2}$ 30 Pa (Ar-O_2)(?)
Kim and Moorhead (1990) [45]	Gravimetry	HIP (+6%Y_2O_3+1.5%Al_2O_3)	H_2-H_2O (P_{total}=0.1 MPa) ($V=9\times10^{-3}$ m$\cdot$s^{-1}) Ar-O_2 (P_{total}=0.1 MPa) ($V=9\times10^{-3}$ m$\cdot$s^{-1})	1673	Linear H_2-H_2O 8×10^{-7} kg$\cdot$m$^{-2}\cdot$s^{-1} (P_{H_2O}=1-10 Pa) 5×10^{-7} kg$\cdot$m$^{-2}\cdot$s^{-1} (P_{H_2O}=100 Pa) Ar-O_2 3×10^{-7} kg$\cdot$m$^{-2}\cdot$s^{-1} (P_{O_2}=1-10 Pa)	$P^t_{O_2}$ 100 Pa (Ar-O_2)
Narushima *et al.* (1994) [56]	Thermogravimetry	CVD (α)	Ar-O_2, N_2-O_2 (P_{total}=0.1 MPa) (P_{O_2}=0.5-120 Pa) ($V=4.87\times10^{-3}$-1.56×10^{-1} m$\cdot$s^{-1})	1823-1923	Linear $4.4\times10^{-6}\{P_{O_2}(\text{atm})\}\times\{V(\text{m}\cdot\text{s}^{-1})\}^{1/2}$ kg$\cdot$m$^{-2}\cdot$s^{-1}	$P^t_{O_2}$ Ar-O_2 1823 K: 16 Pa (1.95×10^{-2} m$\cdot$s^{-1}) 1873 K: 112 Pa (4.87×10^{-3} m$\cdot$s^{-1}) 1873 K: 7.6 Pa (1.56×10^{-1} m$\cdot$s^{-1}) 1923 K: 89 Pa (1.95×10^{-2} m$\cdot$s^{-1}) N_2-O_2 1823 K: 16 Pa (1.95×10^{-2} m$\cdot$s^{-1}) 1923 K: 89 Pa (1.95×10^{-2} m$\cdot$s^{-1})

Table 7 Continued.

Narushima *et al.* (1994) [57]	Thermogravimetry	CVD (α)	CO-CO_2 (P_{total}=0.1 MPa) ($P_{CO_2}/P_{CO}=10^{-4.9}$-$10^{1.1}$) ($V$=4.87×10^{-3}-1.46×10^{-1} m·s^{-1})	1823-1923	Linear 1873 K (1.95×10^{-2} m·s^{-1}) 5.0×10^{-6} kg·m^{-2}·s^{-1} ($P_{CO_2}/P_{CO}=10^{-4}$) 3.2×10^{-6} kg·m^{-2}·s^{-1} ($P_{CO_2}/P_{CO}=10^{-3}$) 1.3×10^{-6} kg·m^{-2}·s^{-1} ($P_{CO_2}/P_{CO}=10^{-2}$) 3.2×10^{-7} kg·m^{-2}·s^{-1} ($P_{CO_2}/P_{CO}=10^{-1}$)	$(P_{CO_2}/P_{CO})^t$ 1873 K: 10^0-10^1

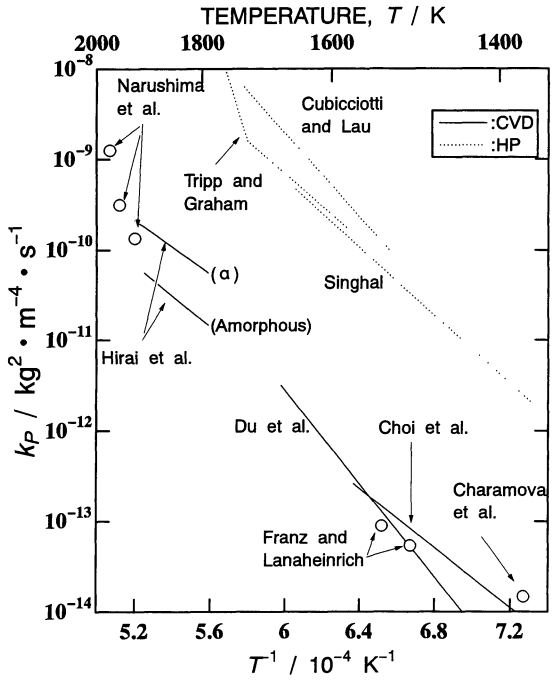

Fig. 10 Comparison of the parabolic rate constants of Si_3N_4 in dry oxygen.

MgO or Y_2O_3 are higher than those of CVD-Si_3N_4 which can form pure silica as oxidation products[135]. It was reported that the rate-controlling step of oxidation for CVD-Si_3N_4 was oxygen diffusion in oxide film[114)-(116)], while the diffusion of cation (Mg^{2+} or Y^{3+}) in Si_3N_4[130)(133)] or the silicate glass film[129] might be the rate-controlling step for HP-Si_3N_4.

Wet oxidation behavior of Si_3N_4 was mainly investigated in the temperature range of 1000 to 1300 K because the purpose of the investigation is its application to electronic devices. In contrast to dry oxidation behavior, linear oxidation was observed in wet atmospheres even at lower temperatures[119)(121)(124)]. Water vapor accelerates the oxidation of Si_3N_4.

Silicon oxynitride (Si_2N_2O) may be formed during oxidation of Si_3N_4 at the Si_3N_4/SiO_2 interface. Du *et al.* detected[116] a duplex oxide scale consisting of SiO_2 and Si_2N_2O after the oxidation of CVD-Si_3N_4 at 1373 to 1673 K by using SIMS and XPS techniques[136]. They concluded that the rate-controlling step of the oxidation was the oxygen diffusion in Si_2N_2O layer according to the low oxidation rates and a high activation energy. The presence of $Si_xN_yO_z$ phase was observed in the oxidation of Si_3N_4 at 1343 to 1413 K by Maguire and Augustus[137] and Raider *et al.*[138]. On the contrary, no Si_2N_2O phase was detected during oxidation of CVD-Si_3N_4 at 1823 to 2003 K[66] by the present authors. Ogbuji *et al.* reported[139)-(141)] that the Si_2N_2O phase was observed between SiO_2 and Si_3N_4 in the oxidation below 1723 K while not above 1773 K.

2. Active oxidation

(1) In low total pressure gas or inert gas-oxygen mixture gas

Si_3N_4 may decompose into Si(l) and N_2(g) as represented by eq. (13) in a low total pressure or an inert gas-oxygen mixture gas at high temperatures.

$$Si_3N_4(s)=3Si(l)+2N_2(g) \quad (13)$$

The equilibrium nitrogen pressure of eq. (13) at 1873 K is calculated to be 2.4×10^3 Pa according to thermodynamic data[43]. However, the decomposition of Si_3N_4 is observed only in the atmosphere with the total gas pressure lower than 10^{-3} Pa at 1673 to 2023 K[142)(143)]. Mass loss of Si_3N_4 is dominated by the active oxidation at the total pressures higher than several Pa[82]. The effect of the decomposition on the mass loss is negligible in an Ar-O_2 mixture gas near atmospheric pressure at 1823 to 1923 K because little mass loss was seen in a pure argon or nitrogen gas and the mass loss rate was proportional to the ambient oxygen partial pressure[56]. The rate-controlling step of active oxidation of Si_3N_4 in a low total pressure gas or an inert gas-oxygen mixture gas was oxygen diffusion through a gaseous boundary layer[56]. The active oxidation rates of Si_3N_4 normalized by the oxygen consumption were comparable to those of SiC[56].

Figure 11 summarizes the reported $P^t_{O_2}$ values of Si_3N_4. $P^t_{O_2}(W_A)$ and $P^t_{O_2}(W_B)$ in Fig. 11 are the $P^t_{O_2}$ values calculated from Wagner model for $P_{N_2}=10^5$ and 10^2 Pa, respectively. The $P^t_{O_2}$ values reported by Vaughn and Maahs[82] and Warburton[118] agreed well with the estimation from Wagner model. The effect of SiO_2 smoke formation (eq. (9)) on the active-to-passive transition might be small in low total gas pressure atmospheres.

Sheehan demonstrated[126] that HP-Si_3N_4 bodies containing higher MgO impurity levels had higher $P^t_{O_2}$ values. Kim and Moorhead[45] reported that no mass loss was observed for CVD-Si_3N_4 and a significant amount of mass loss for HIP (hot isostatic pressed)-Si_3N_4 at 1673 K in Ar-O_2 atmospheres (total pressure=0.1 MPa). Impuri-

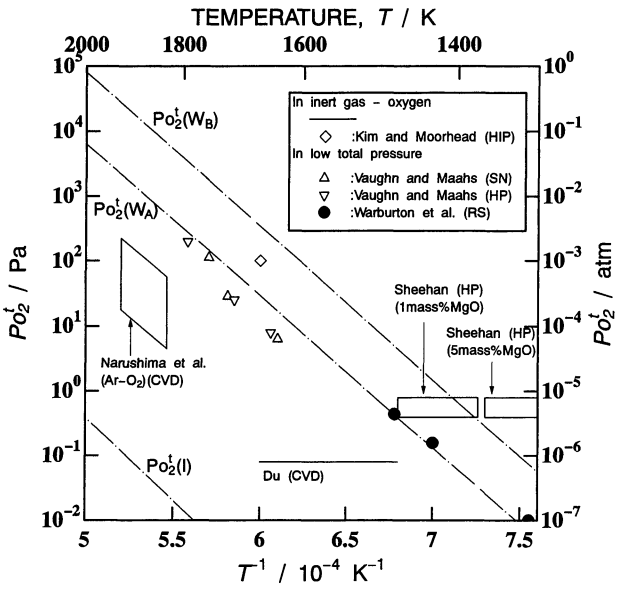

Fig. 11 Comparison of the active-to-passive transition oxygen partial pressure of Si_3N_4.

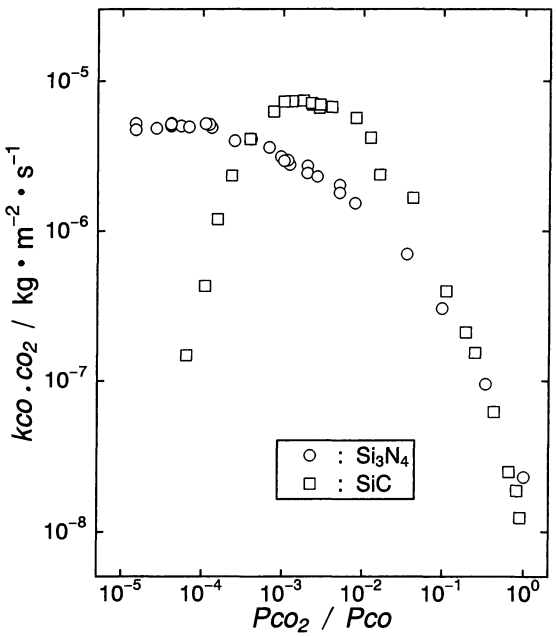

Fig. 12 Comparison of the active oxidation rates ($k_{CO\cdot CO_2}$) between CVD-SiC and CVD-Si_3N_4 in CO-CO_2 atmospheres.

ties in Si_3N_4 bodies may increase the $P^t_{O_2}$ value.

(2) In CO-CO_2 or H_2-H_2O atmosphere

In a higher oxygen potential region, the formation of SiO_2 by oxidation of Si_3N_4 and the reduction of the SiO_2 to SiO gas were observed during active oxidation of Si_3N_4 in a CO-CO_2 and in an H_2-H_2O atmosphere[57][127].

In a lower oxygen potential region of a CO-CO_2 atmosphere ($P_{CO_2}/P_{CO}<10^{-4}$), carbon particles were formed on the surface as an oxidation product. A chemical reaction between Si_3N_4 and CO may be rate controlling. Kim reported[127] that the decomposition of Si_3N_4 (eq. (13)), not active oxidation, occurred in a lower oxygen potential region of an H_2-H_2O atmosphere, but the experimental evidence of the decomposition was not shown.

The active oxidation rates of CVD-Si_3N_4 are compared with those of CVD-SiC at 1873 K in CO-CO_2 atmospheres in Fig. 12[57]. Since the rate-controlling step of the active oxidation in the region of $P_{CO_2}/P_{CO}>10^{-1}$ is the diffusion of gas species formed by the reduction of SiO_2(eq. (12)) for both of CVD-Si_3N_4 and CVD-SiC, the active oxidation rate of CVD-Si_3N_4 is almost in agreement with that of CVD-SiC. In the region of $P_{CO_2}/P_{CO}<10^{-3.5}$, the active oxidation rates of CVD-Si_3N_4 are larger than those of CVD-SiC. This may be caused by the difference of the oxidants, CO gas for CVD-Si_3N_4 and CO_2 gas for CVD-SiC. For P_{CO_2}/P_{CO} around 10^{-3}, the carbon formed on the surface of CVD-SiC may accelerate the reduction of SiO_2 (eq. (12)), and the active oxidation rates of CVD-SiC are larger.

V. Summary

Two kinds of oxidation behavior of SiC and Si_3N_4, passive and active oxidation, at high temperatures were reviewed. Passive oxidation behavior was affected by the microstructure of oxide films formed during the oxidation process. SiO gas pressure on the surface of SiC and Si_3N_4 was the dominant factor in active oxidation. Wagner model, volatility diagram and solgasmix-based calculation could well explain the active-to-passive transition which was important for the practical use of silicon-based ceramics.

Experimental and theoretical studies on the oxidation are expected by using the new analytical techniques and computer simulation in addition to the basic research on oxide film and behavior of gas species in oxide for further understanding of the oxidation of silicon-based ceramics.

REFERENCES

(1) K. Komeya: Bull. Ceram. Soc. Jpn., **25** (1990), 35.
(2) R. W. Ohnsorg and M. O. Ten Eyck: *Silicon Carbide 1987*, Ed. by J. D. Cawley and C. E. Semier, Am. Ceram. Soc., Westerville, OH, (1989), p. 367.
(3) Y. Naruse and T. Hatta: Bull. Ceram. Soc. Jpn., **18** (1983), 42.
(4) S. Y. Dapkunas: Ceramic Bull., **67** (1988), 388.
(5) J. W. MacBeth: Ceramic Bull., **71** (1992), 174.
(6) H. Kinugasa: Bull. Ceram. Soc. Jpn., **18** (1983), 47.
(7) H. Ohno: Bull. Ceram. Soc. Jpn., **23** (1988), 656.
(8) J. Chin and T. Ohkawa: Nucl. Tech., **32** (1977), 115.
(9) T. Iseki: Bull. Ceram. Soc. Jpn., **21** (1986), 510.
(10) Y. Hirohata, M. Kobayashi, S. Maeda, K. Nakamura, M. Mohri, K. Watanabe and T. Yamashita: Thin Solid Films, **63** (1979), 237.
(11) R. A. L. Drew: Can. Metall. Qurt., **27** (1988), 59.
(12) K. Koga: Bull. Ceram. Soc. Jpn., **25** (1990), 107.
(13) M. Sasaki: Bull. Ceram. Soc. Jpn., **25** (1990), 225.
(14) O. Kamigaito: Bull. Ceram. Soc. Jpn., **25** (1990), 225.
(15) N. N. Ault: Ceram. Bull., **70** (1991), 882.
(16) T. Itoh: Bull. Ceram. Soc. Jpn., **23** (1988), 638.
(17) Y. Hattori: Kinou Zairyo 1989, No. 8 (1989), 32.
(18) Am. Ceram. Soc. Bull., **65** (1986), 342-376.
(19) Am. Ceram. Soc. Bull., **66** (1987), 330-352.
(20) A. K. Misra: J. Mat. Sci., **26** (1991), 6591.

(21) M. Backhaus-Ricoult: J. Am. Ceram. Soc., **74** (1991), 1793.
(22) K. W. White and L. Gauzzone: J. Am. Ceram. Soc., **74** (1991), 2280.
(23) M. Sasaki: Ph.D Thesis, Tohoku Univ., (1991).
(24) W. v. Munch and P. Hoeck: Solid State Electron., **21** (1978), 479.
(25) S. Nishino, A. Ibaraki, H. Matsunami and T. Tanaka: Jpn. J. Appl. Phys., **19** (1980), 353.
(26) S. Nishino, J. A. Powell and H. A. Will: Appl. Phys. Lett., **42** (1983), 460.
(27) K. Shibahara, S. Nishino and M. Matsunami: Jpn. J. Appl. Phys., **23** (1984), 862.
(28) S. Yoshida, K. Sasai, E. Sakura, S. Misawa and S. Gonda: Appl. Phys. Lett., **46** (1985), 766.
(29) S. Yoshida, H. Daimon, M. Yamanaka, E. Sakuma, S. Misawa and K. Endo: J. Appl. Phys., **60** (1986), 2989.
(30) J. W. Palmour, H. S. Kong and R. F. Davis: Appl. Phys. Lett., **51** (1987), 2028.
(31) M. Kuwagaki, K. Imai, T. Ogino and Y. Amemiya: Jpn. J. Appl. Phys., **28** (1989), 173.
(32) M. Shinohara, M. Yamanaka, S. Misawa, H. Okumura and S. Yoshida: Jpn. J. Appl. Phys., **30** (1991), 240.
(33) T. Yoshimi and H. Katoh: Bull. Ceram. Soc. Jpn., **20** (1985), 280.
(34) S. C. Singhal: Ceram. Int., **2** (1976), 123.
(35) S. C. Singhal: *Properties of High Temperature Alloys.* Ed. by Z. A. Foroulis and F. S. Pettit, The Electrochem. Soc., Princeton, NJ, (1976), p. 697.
(36) A. C. Lea: J. Soc. Glass Technol., **33** (1949), 27.
(37) G. Ervin, Jr.: J. Am. Ceram. Soc., **41** (1958), 347.
(38) H. Suzuki: J. Ceram. Soc. Jpn., **67** (1959), 157.
(39) P. J. Jorgensen, M. E. Wadsworth and I. B. Cutler: J. Am. Ceram. Soc., **43** (1960), 209.
(40) J. Schlichting: Ber. Dt. Keram. Soc., **56** (1979), 196.
(41) J. Schlichting: Ber. Dt. Keram. Soc., **56** (1979), 256.
(42) N. S. Jacobson: J. Am. Ceram. Soc., **76** (1993), 3.
(43) O. Kubaschewski and C. B. Alcock: *Metallurgical Thermochemistry 5th ed.*, Pergamon Press, New York, (1979), p. 378.
(44) H. E. Kim and A. J. Moorhead: J. Am. Ceram. Soc., **73** (1990), 1868.
(45) H. E. Kim and A. J. Moorhead: J. Am. Ceram. Soc., **73** (1990), 3007.
(46) C. Wagner: J. Appl. Phys., **29** (1958), 1295.
(47) E. T. Turkdogan, P. Grievson and L. S. Darken: J. Phys. Chem., **67** (1963), 1647.
(48) K. G. Nickel: J. Euro. Ceram. Soc., **9** (1992), 3.
(49) O. Kubaschewski and C. B. Alcock: *Metallurgical Thermochemistry 5th ed.*, Pergamon Press, New York, (1979), p. 221.
(50) T. Rosenqvist and J. KR. Tuset: Metall. Trans. B, **18B** (1987), 471.
(51) V. L. K. Lou and T. E. Mitchell and A. H. Heuer: J. Am. Ceram. Soc., **68** (1985), 49.
(52) V. L. K. Lou and A. H. Heuer: *High Temperature Corrosion of Technical Ceramics*, Ed. by R. J. Fordham. Elsevier Applied Science, England, (1990), 33.
(53) A. H. Heuer and V. L. K. Lou: J. Am. Ceram. Soc., **73** (1990), 2789.
(54) G. Eriksson and K. Hack: Metall. Trans. B, **21B** (1990), 1013.
(55) T. Narushima, T. Goto, Y. Iguchi and T. Hirai: J. Am. Ceram. Soc., **74** (1991), 2583.
(56) T. Narushima, T. Goto, Y. Yokoyama, J. Hagiwara, Y. Iguchi and T. Hirai: J. Am. Ceram. Soc., **77** (1994), 2369.
(57) T. Narushima, T. Goto, J. Hagiwara, Y. Iguchi and T. Hirai: J. Am. Ceram. Soc., **77** (1994), 2921.
(58) E. A. Gulbransen, K. F. Andrew and F. A. Brassart, J. Electrochem. Soc., **113** (1966), 1311.
(59) R. W. Bartlett, J. Electrochem. Soc., **118** (1971), 397.
(60) R. C. A. Harris and R. L. Call: *Silicon Carbide 1973*, Ed. by R. C. Marchall, J. W. Faust, Jr. and C. E. Ryan. University of South Carolina Press, Columbia, SC, (1974), p. 329.
(61) R. Kossowski and S. C. Singhal: *Grain Boundary in Engineering Materials*, Ed. by J. J. Walter, J. H. Westbrook and D. A. Woodford, Baton Rouge, NY, (1975), p. 257.
(62) J. A. Costello and R. E. Tressler: J. Am. Ceram. Soc., **69** (1986), 674.
(63) T. Narushima, T. Goto and T. Hirai: J. Am. Ceram. Soc., **72** (1989), 1386.
(64) Z. Zheng, R. E. Tressler and K. E. Spear: J. Electrochem. Soc., **137** (1990), 854.
(65) F. Sibieude, J. Rodriguez and M. T. Clavaguera-mora: Thin Solid Films, **204** (1991), 217.
(66) T. Narushima, R. Y. Lin, Y. Iguchi and T. Hirai: J. Am. Ceram. Soc., **76** (1993), 1047.
(67) G. Q. Weaver and B. A. Olson: *Silicon Carbide 1973*, Ed. by R. C. Marchall, J. W. Faust, Jr. and C. E. Ryan, University of South Carolina Press, Columbia, SC, (1974), p. 367.
(68) S. C. Singhal: J. Am. Ceram. Soc., **59** (1976), 81.
(69) A. Suzuki, H. Ashida, N. Furui, K. Mameno and H. Matsunami: Jpn. J. Appl. Phys., **21** (1982), 579.
(70) W. J. Lu, A. J. Steckl, T. P. Chow and W. Katz: J. Electrochem. Soc., **131** (1984), 1907.
(71) C. D. Fung and J. J. Kopanski: Appl. Phys. Lett., **45** (1984), 757.
(72) R. E. Tressler, J. A. Costello and Z. Zheng: *Industrial Heat Exchangers*, Ed. by Dr. Hayes *et al.*, Am. Soc. Metals, (1985), p. 307.
(73) M. Maeda, K. Nakamura and T. Ohkubo: J. Mat. Sci., **23** (1988), 3933.
(74) T. Narushima, T. Goto, Y. Iguchi and T. Hirai: J. Am. Ceram. Soc., **73** (1990), 3580.
(75) E. J. Opila: J. Am. Ceram. Soc., **77** (1994), 730.
(76) D. E. Rosner and H. D. Allendorf: J. Phys. Chem., **74** (1970), 1829.
(77) J. E. Antill and J. B. Warburton: Corr. Sci., **11** (1971), 337.
(78) V. I. Elchin, B. V. Lukin, A. E. Rautbout, A. I. Rekov, V. E. Serebrennikova, I. A. Yovorskii, G. E. Val'yano and M. D. Malanov: Izvest. Akad. Nauk. SSSR, Neorgan. Mater., **7** (1971), 1342.
(79) M. J. Bennett and G. H. Chaffey: J. Nucl. Mat., **52** (1974), 184.
(80) J. W. Hinze and H. C. Graham: J. Electrochem. Soc., **123** (1976), 1066.
(81) H. E. Kim and D. W. Readey: *Silicon Carbide 1987*, Ed. by J. D. Cawley and C. E. Semier, Am. Ceram. Soc., Westerville, OH, (1989), p. 301.
(82) W. L. Vaughn and H. G. Maahs: J. Am. Ceram. Soc., **73** (1990), 1540.
(83) N. S. Jacobson, A. J. Eckel, A. K. Misra and D. L. Humphrey: J. Am. Ceram. Soc., **73** (1990), 2330.
(84) D. P. Butt, R. E. Tressler and K. E. Spear: J. Am. Ceram. Soc., **74** (1991), 457.
(85) M. Balat, G. Flamant, G. Male and G. Pichelin: J. Mat. Sci., **27** (1992), 697.
(86) D. P. Butt, R. E. Tressler and K. E. Spear: J. Am. Ceram. Soc., **75** (1992), 3257.
(87) T. Narushima, T. Goto, Y. Yokoyama, Y. Iguchi and T. Hirai: J. Am. Ceram. Soc., **76** (1993), 1047.
(88) T. Narushima, T. Goto, Y. Yokoyama, M. Takeuchi, Y. Iguchi and T. Hirai: J. Am. Ceram. Soc., **77** (1994), 1079.
(89) E. M. Levin, C. R. Robbins and H. F. McMurdie, *Phase Diagram for Ceramists, 1969 Supplement*, The Am. Ceram. Soc., Columbus, OH, (1969), p. 76.
(90) S. C. Singhal and F. F. Lange: J. Am. Ceram. Soc., **58** (1975), 433.
(91) J. W. Hinze, W. C. Tripp and H. C. Graham: *Mass Transport Phenomena in Ceramics*, Ed. by A. R. Cooper and A. H. Heuer, Plenum Publ., NY, (1975), 409.
(92) S. C. Singhal: J. Mat. Sci., **11** (1976), 1246.
(93) J. Schlichting and K. Schwetz: High Temp. High Press., **14** (1982), 219.
(94) I. A. Aksay and J. A. Pask: J. Am. Ceram. Soc., **58** (1975), 507.
(95) N. G. Ainslie, C. R. Morelock and D. Turnbull: *Symposium on Nucleation and Crystallization in Glasses and Melts*, Ed. by M.

K. Reser, G. Smith and H. Insley., The Am. Ceram. Soc., Columbus, OH, (1962), p. 97.
(96) W. D. Kingary: *Introduction to Ceramics*, Wiley & Sons, NY, (1960), p. 137.
(97) L. U. Ogbuji: J. Mat. Sci., **16** (1981), 2753.
(98) A. H. Heuer, L. U. Ogbuji and T. E. Mitchell: J. Am. Ceram. Soc., **63** (1980), 354.
(99) J. A. Costello and R. E. Tressler: J. Am. Ceram. Soc., **64** (1981), 327.
(100) K. L. Luthra: J. Am. Ceram. Soc., **74** (1991), 1095.
(101) G. H. Schiroky: Ad. Ceram. Mat., **2** (1987), 137.
(102) A. J. Moulson and J. P. Roberts: Trans. Faraday Soc., **57** (1961), 1208.
(103) S. Rigo, F. Rochet, A. Agius and A. Straboni: J. Electrochem. Soc., **129** (1982), 867.
(104) S. Ban-ya, Y. Iguchi and S. Yamamoto: Tetsu-to-Hagané, **72** (1986), 2210.
(105) H. Cappelen, K. H. Johansen and K. Motzfeldt: Acta Chemica Scand., **A 35** (1981), 247.
(106) E. A. Irene and R. Ghez: J. Electrochem. Soc., **124** (1977), 1757.
(107) F. E. Wagstaff, S. D. Brown and I. B. Cutler: Phys. Chem. Glass., **5** (1964), 76.
(108) F. E. Wagstaff and K. J. Richards: J. Am. Ceram. Soc., **49** (1966), 118.
(109) I. Franz and W. Langheinrich: Solid-State Electron., **14** (1971), 499.
(110) J. H. Rosolowski and C. D. Greskovich: Semi-Annual Tech. Rept., ARPA Order No. 2698, Program No. 4D10, Advanced Research Projects Agency, Office of Naval Research, Arlington, Virginia, Oct. (1974).
(111) H. Mellottee, G. Cochet and R. Delbourgo: Revue de Chimie Minerale, **13** (1976), 373.
(112) T. Enomoto, R. Ando, H. Morita and H. Nakayama: Jpn. J. Appl. Phys., **17** (1978), 1049.
(113) F. S. Galasso, R. D. Veltri and W. J. Croft: Am. Ceram. Soc. Bull., **57** (1978), 453.
(114) T. Hirai, K. Niihara and T. Goto: J. Am. Ceram. Soc., **63** (1980), 419.
(115) L. V. Chramova, T. P. Smirnova, B. M. Ayupov and V. I. Belyi: Thin Solid Films, **78** (1981), 303.
(116) H. Du, R. E. Tressler, K. E. Spear and C. G. Pantano: J. Electrochem. Soc., **136** (1989), 1527.
(117) D. J. Choi, D. B. Fischbach and W. D. Scott: J. Am. Ceram. Soc., **72** (1989), 1118.
(118) J. B. Warburton, J. E. Antill and W. M. Hawes: J. Am. Ceram. Soc., **61** (1978), 67.
(119) J. C-H. Hui, T-Y. Chiu, S-W. Wong and W. G. Oldman: IEEE Trans. Electron Devices, **ED-29** (1982), 554.
(120) T. Sato, K. Haryu, T. Endo and M. Shimada: J. Mater. Sci., **22** (1987), 2635.
(121) A. E. T. Kuiper, M. F. C. Willemsen and J. M. L. Mulder: J. Vac. Sci. Technol., **B7** (1989), 455.
(122) M. Maeda, K. Nakamura and M. Yamada: J. Mater. Sci., **25** (1990), 3790.
(123) A. Fourrier, A. Bosseboeuf, D. Bouchier and G. Gautherin: J. Electrochem. Soc., **138** (1991), 1084.
(124) T. Narushima, Y. Iguchi, H. Tagawa, T. Hayashi, T. Goto and T. Hirai: Collected Abstracts of 1994 Spring Meeting of Japan Inst. Metals, p. 340.
(125) W. C. Tripp and H. C. Graham: J. Am. Ceram. Soc., **59** (1976), 399.
(126) J. E. Sheehan: J. Am. Ceram. Soc., **65** (1982), C111.
(127) H. E. Kim: Ph.D Thesis, The Ohio State Univ., Columbus, OH, (1987).
(128) H. Du: Ph.D Thesis, Pennsylvania State University, (1988).
(129) S. C. Singhal: J. Mat. Sci., **11** (1976), 500.
(130) D. Cubiccioti and K. H. Lau: J. Am. Ceram. Soc., **61** (1978), 512.
(131) E. M. Levin, C. R. Robbins and H. F. McMurdie: *Phase Diagram for Ceramists, 1969 Supplement*, The Am. Ceram. Soc., Columbus, OH, (1969), p. 88 and p. 107.
(132) J. Schlichting and J. Gauckler: Pow. Metall. Int., **9** (1977), 36.
(133) D. M. Mieskowski and W. A. Sanders: J. Am. Ceram. Soc., **68** (1985), C160.
(134) K. Yonezawa: Master Thesis, Tohoku University, (1985).
(135) J. Schlichting: High Temp. High Press., **14** (1982), 717.
(136) R. K. Brow and C. G. Pantano: J. Am. Ceram. Soc., **69** (1986), 314.
(137) H. G. Maguire and P. D. Augustus: J. Electrochem. Soc., **119** (1972), 791.
(138) S. I. Raider, R. Flitsch, J. A. Aboaf and W. A. Pliskin: J. Electrochem. Soc., **123** (1976), 560.
(139) L. U. J. T. Ogbuji: J. Am. Ceram. Soc., **75** (1992), 2995.
(140) L. U. T. Ogbuji and D. T. Jayne: J. Electrochem. Soc., **140** (1993), 759.
(141) L. U. J. T. Ogbuji and J. L. Smialek: J. Electrochem. Soc., **138** (1991), L51.
(142) H. D. Batha and E. D. Whitney: J. Am. Ceram. Soc., **56** (1973), 365.
(143) T. Goto and T. Hirai: J. Mat. Sci., **22** (1987), 2842.